

Hyperthermia Reduces Irradiation-Induced Tumor Repopulation in an In Vivo Pancreatic Carcinoma Model

Patrizia Sarogni, Agata Zamborlin, Ana Katrina Mapanao, Tine Logghe, Luigi Brancato, Eke van Zwol, Michele Menicagli, Noemi Giannini, Alessandra Gonnelli, Stefania Linsalata, Robin Colenbier, Johan Van den Bossche, Fabiola Paiair, Johannes Bogers,* and Valerio Voliani*

Pancreatic cancer has a poor prognosis due to its aggressive nature and ability to metastasize at an early stage. Currently, its management is still a challenge because this neoplasm is resistant to conventional treatment approaches, among which is chemo-radiotherapy (CRT), due to the abundant stromal compartment involved in the mechanism of hypoxia. Hyperthermia, among other effects, counteracts hypoxia by promoting blood perfusion and thereby can enhance the therapeutic effect of radiotherapy (RT). Therefore, the establishment of integrated treatments would be a promising strategy for the management of pancreatic carcinoma. Here, the effects of joint radiotherapy/hyperthermia (RT/HT) on optimized chick embryo chorioallantoic membrane (CAM) pancreatic tumor models are investigated. This model enables a thorough assessment of the tumor-arresting effect of the combined approach as well as the quantitative evaluation of hypoxia and cell cycle-associated mechanisms by both gene expression analysis and histology. The analysis of the lower CAM allows to investigate the variation of the metastatic behaviors of the cancer cells associated with the treatments. Overall, this study provides a potentially effective combined strategy for the non-invasive management of pancreatic carcinoma.

1. Introduction

The survival rate for pancreatic cancer patients is still limited, with a 5-year survival in only 9% of cases, despite improvements in the management of cancer therapy.^[1] The lack of symptoms and the non-specificity of diagnostic tests at the early stages of the disease are the major causes of cancer progression to advanced stages.^[2] Surgery, chemotherapy (CT), and radiotherapy (RT) are the first-line treatments to improve both patient outcome and quality of life. However, there is still no definitive cure for this malignancy at metastatic stage.^[3] Current treatments which have shown promising but limited results in patients with locally advanced or metastatic pancreatic cancer include a multi-agent regimen, such as FOLFIRINOX (leucovorin, fluorouracil, irinotecan, and oxaliplatin), GEMOXEL (gemcitabine, oxaliplatin, and


P. Sarogni, A. Zamborlin, A. K. Mapanao, N. Giannini, A. Gonnelli, V. Voliani

Center for Nanotechnology Innovation@NEST
Istituto Italiano di Tecnologia
Piazza San Silvestro 12, Pisa 56127, Italy
E-mail: valerio.voliani@unige.it

A. Zamborlin
NEST-Scuola Normale Superiore
Piazza San Silvestro 12, Pisa 56127, Italy

T. Logghe, L. Brancato, E. van Zwol, J. Van den Bossche, J. Bogers
ElmediX NV
Dellingstraat 34-1, Mechelen 2800, Belgium
E-mail: john-paul.bogers@elmedix.com, eke.vanzwol@elmedix.com

M. Menicagli
Fondazione Pisana per la Scienza ONLUS
via Ferruccio Giovannini 13, S. Giuliano Terme, Pisa 56017, Italy

 The ORCID identification number(s) for the author(s) of this article can be found under <https://doi.org/10.1002/adbi.202200229>.

© 2023 The Authors. Advanced Biology published by Wiley-VCH GmbH. This is an open access article under the terms of the Creative Commons Attribution License, which permits use, distribution and reproduction in any medium, provided the original work is properly cited.

DOI: 10.1002/adbi.202200229

N. Giannini, A. Gonnelli, F. Paiair
Radiation Oncology Unit
Pisa University Hospital "Azienda Ospedaliero-Universitaria Pisana"
Via Roma 67 56126, Pisa, Italy

S. Linsalata
Unit of Medical Physics
Pisa University Hospital "Azienda Ospedaliero-Universitaria Pisana"
Pisa 56126, Italy

R. Colenbier, J. Bogers
University of Antwerp
Laboratory of Cell Biology and Histology
University of Antwerp
Antwerpen 2610, Belgium

V. Voliani
Department of Pharmacy
University of Genoa
Viale Cembrano, 4, Genoa 16148, Italy

A. K. Mapanao
Center for Radiopharmaceutical Sciences
Paul Scherrer Institute
5232 Villigen-PSI, Forschungsstrasse, Switzerland

capecitabine), and cisplatin/epirubicin/5FU/gemcitabine.^[4] The complexity of these combinations of drugs increases the side effects without significantly overcoming the pancreatic cancer resistance, which is largely promoted by the tumor micro-environment (TME) and oxygen deprivation.^[5] Such hypoxic environment hampers the delivery of drugs or the effects of RT, decreasing the sensitivity of the malignancy to both CT and RT, and subsequently resulting in a negative prognosis.^[6] Therefore, new therapeutic strategies to reduce tumor resistance are increasingly demanded.

The application of heat in cancer treatment is better known as hyperthermia (HT) or thermal treatment, in which the mean patient temperature is elevated above normal range. Beyond local- and regional-, whole-body HT (WBH) is the only treatment modality that has the potential to act on both primary tumor and distant metastases.^[7] Besides, WBH has been shown to be a powerful adjuvant to chemo- and radiotherapy by inducing changes in the oxidative metabolism, thereby sensitizing cancer cells to the cytotoxic effects of these treatment modalities. In the last decades, several devices, technology platforms, and procedures to apply heat and heating protocols have been developed. Achievement of an effective treatment requires high quality heating equipment, precise thermal dosimetry, and adequate quality assurance.^[8]

In this context, properly designed combinatorial treatment strategies can give rise to significant advances in pancreatic cancer management.

This work investigates the effects of controlled HT on pancreatic ductal adenocarcinoma (PDAC) treated in combination with RT. The evaluations have been performed on optimized pancreatic carcinoma chick embryo chorioallantoic membrane (CAM) models, an *in vivo* system that provides a suitable environment to support tumor growth in agreement to the European Parliament Directive 2010/63/EU¹⁴. The employment of the CAM tumor model finds increasing importance for the investigation of various therapeutic strategies in oncological research.^{13,38,39} The direct monitoring of tumor growth provides rapid assessment of potential tumor-reducing effect and morphological alteration following the treatment.^[9] Thus, growing evidence of the applicability of this *in vivo* model in exploring the efficacy of drug delivery-based therapies, angiogenesis inhibition, targeted-therapies and nanomaterial-based approaches increasingly encourages the use of the CAM model in the preclinical research workflow.^[10–13] Besides providing a combined approach for the non-invasive management of pancreatic carcinoma, our study further supports the significance of CAM tumor models in oncological research for the assessment of conventional and emerging treatment strategies as well as for the comprehension of the molecular mechanisms involved in tumor treatment response.

2. Experimental Section

2.1. 2D Cell Culture

The human pancreatic cancer cell line BxPC-3 (ATCC CRL-1687) was purchased from American Type Culture Collection (ATCC). BxPC-3 cells were cultured in RPMI 1640 medium (Gibco 11875093) supplemented with 10% FBS, 1 mM sodium

pyruvate (Gibco 11360070), and 1× penicillin–streptomycin (equivalent to 50 U mL⁻¹; Gibco 15140-122). Cells were maintained in an incubator set at 37 °C and 5% CO₂.

2.2. Chorioallantoic Membrane Assay (CAM) Tumor Model

CAM models of pancreatic carcinoma have been produced through the authors' standard protocol.^[14] Fertilized red Leghorn eggs were purchased from a local supplier and immediately stored at 4 °C upon delivery. Before incubation, at Embryonic Day of Development (EDD) 0, the eggs were cleaned with deionized water and placed in trays inserted in a fan-assisted incubator (FIEM MG 140/200) set at 37.5 °C with ≈47% humidity. Eggs were punctured on EDD3 and tumor pancreatic cells (3 × 10⁶ BxPC-3 cells) were inoculated on the CAM at EDD6. Eggs were incubated for 4 days and randomized into six different treatment groups. In particular, i) two groups received RT alone at a dose of 1 and 2 Gy respectively, both on EDD12 and EDD14; ii) two groups received RT (1 or 2 Gy) on EDD12 and EDD14 and HT, administered on EDD10, 12, and 14; and iii) one normothermic (37 °C) and one hyperthermic (41.5 °C) condition. Heat treatment (HT, 41.5 °C for 6 h) was administered with a customized heating device (Egg incubator, ElmediX). During the treatment, a humidity of 47% was maintained. The radiotherapy treatment (RT) was performed through a Varian Clinac DHX linear accelerator. The tumor dimension before and after treatment was measured using a portable digital microscope. The volumes were derived using the formula $\frac{1}{2}(\text{length} \times \text{width}^2)$, where the length and width corresponded to the largest and smallest diameter, respectively. On EDD15, the experiment was concluded, and tumors were harvested for following biological end-point analysis. The different combinations of treatments were investigated to determine a suitable strategy for pancreatic cancer management by evaluating the effects on tumor volume, molecular mechanisms involved in gene expression regulation, and the response to the metastatic ability of BxPC-3 cancer cells.

2.3. Hematoxylin and Eosin (H&E) Staining

Tissues (liver, lung, and tumor) were fixed in 10% buffered formalin. Sections of 4 μm thickness were obtained from paraffin blocks using a microtome (Leica RM2255 Germany) and stained with hematoxylin-eosin (H&E). Samples were dewaxed with xylene and dehydrated in ethanol dilutions. This was followed by staining with hematoxylin for 5 min (Mayer hematoxylin, Diapath C0303) and with eosin for 1 min (Eosin G o Y alcoholic 0.5% Diapath C0353). Thereafter, they were re-immersed in ethanol and xylene. Slides were mounted using a synthetic mounting medium (Thermoscientific, LAMPB/DPX).

2.4. Immunohistochemistry (IHC)

Deparaffinized samples were treated for 10 min with hydrogen peroxide solution (3%) to stop endogenous peroxidase activity. Thereafter, samples were immersed in EDTA-based buffer (pH 8.0) (Leica Biosystems RE7116-CE) and heated in a microwave

oven (10 min, 480 W) for antigen retrieval. Non-specific staining was prevented with blocking peptide (Abcam HRP/DAB, detection kit, ab 64261). The primary antibodies for Ki67 (rabbit monoclonal Invitrogen MA5-14520, diluted 1:100), cleaved caspase-3 (rabbit polyclonal Cell Signaling Technology, 9661; diluted 1:200), and TfR (rabbit polyclonal SAB4200398 Sigma-Aldrich, diluted 1:200) were applied and the samples were kept overnight at 4 °C. The detection was performed using the streptavidin–biotin technique (Abcam HRP/DAB, detection kit, ab 64261). Last, the chromogen (diaminobenzidine) was used for IHC development and Mayer's hematoxylin for the counterstaining. A specific algorithm (Positive Pixel Count) was used to quantitatively determine the protein expression of Ki67 and cleaved caspase-3 and IHC images were processed by averaging the signal intensity of three different areas of the slide section. Therefore, a scoring system was automatically assigned to three different classes of positive signal intensity, classifying them into: weak, moderate, and strong.

2.5. RNA Extraction – qPCR

The harvested tumors were minced into pieces using a plastic pestle, whereafter RNA was extracted using a Nucleospin RNA plus kit (MACHEREY-NAGEL 740984.50) following manufacturer's instructions. The extracted RNA samples were quantified using a UV5Nano (Mettler–Toledo), and were then immediately processed or stored at –80 °C. The quality of RNA and efficiency of the extraction procedure were evaluated through agarose gel electrophoresis. RNA (500 ng) was reverse transcribed for cDNA synthesis using an iScript cDNA Synthesis Kit (Biorad 1708891). Then, the total cDNA (500 ng) was diluted to 1:10 in nuclease-free water. Quantitative real-time polymerase chain reaction (qRT-PCR) was performed with iTaq Universal SYBR Green Supermix (Biorad 1725121). PCR samples were prepared with a final volume of 10 µL, with 2.5 ng of cDNA template (1 µL cDNA). Glyceraldehyde 3-phosphate dehydrogenase (GAPDH) was used as housekeeping gene and served as loading control. The sequences of forward and reverse primers used in this study are listed in **Table 1**.

All samples were analyzed in duplicate. The amplification curves were visualized using SYBR Green Analysis on Applied Biosystems Instrument (7300). The recommended thermal cycling program for amplification was as follows: 95 °C for 10 min and 40 cycles at 95 °C for 15 s; 60 °C for 30 s, and 72 °C for 30 s. Relative gene expression levels were calculated using $2^{-\Delta\Delta C_t}$ method.^[15]

Table 1. Primer sequences for qRT-PCR.

Primer	Sequence (5' → 3')
CAIX forward	CCTCAAGAACCCAGAAATATGC
CAIX reverse	CCTCCATAGCGCAATGACT
PCNA forward	CGGATACCTTGGCGCTAGTA
PCNA reverse	CACTCCGCTCTTTGCACAGG
Caspase-3 forward	CAAACCTTTTCAGAGGGGATCG
Caspase-3 reverse	GCATACTGTTTCAGCATGGCAC
GAPDH forward	AGAAGGCTGGGCTCATT
GAPDH reverse	AGTCTTCTGGTGGCAGTGAT

2.6. DNA Extraction – *Alu* PCR

The harvested lower CAM samples were immediately processed or stored at –80 °C. The DNA was extracted using Nucleospin (MACHEREY-NAGEL 740100.250) following the manufacturer's instruction. To facilitate the enzymatic lysis, the tissues were mechanically homogenized with a plastic pestle. Samples were then incubated with the lysis buffer and 10 µL of proteinase K (1–3%) for 1 h at 56 °C on a thermal shaker at maximum speed. The extracted lysate was loaded onto a column to isolate the DNA, which was then eluted with 200 µL of elution buffer. The extracted DNA was quantified using a UV5Nano (Mettler–Toledo) and its integrity was further evaluated through agarose gel electrophoresis. The DNA samples were either immediately processed or stored at 4 °C. To detect human cells in chick tissues, 30 ng of total DNA was used for the amplification of *Alu* sequences with forward primer: 5'-CAGGCGGATCATGAG-GTCAG-3'; reverse primer: 5'-CAGTGGCGTGATCTCAGCTC-3'). The qRT-PCR was performed using the Ssdo Advanced Sybr Green (BIORAD 1725271) and PCR samples were prepared with a final volume of 10 µL. The recommended thermal cycling program for amplification of *Alu* sequences was as follows: 98 °C for 5 min and 40 cycles of 98 °C for 15 s, 60 °C for 30 s, and 72 °C for 30 s. The amplification curves were visualized using SYBR Green Analysis on Applied Biosystems Instrument (7300). The approximate number of human cells in the lower CAM was obtained through a linear equation by increasing the number (10 to 100 000) of human cells per tissue.

2.7. Statistical Analysis

For tumor volume analysis, each single tumor at the specified EDD was normalized over the pretreatment tumor volume at EDD10. Thus, the tumor volume fold change of a specific experimental condition was derived as a ratio over the pretreatment tumor size in Figure S1, Supporting Information. The tumor volume fold change was calculated as a ratio over the average volume fold change of the control at EDD12. Data of the tumor volume were reported as mean ± SD, with at least eight tumor samples per condition. For RT-PCR, data were reported as mean ± SD of three biological replicates and statistical differences were calculated using the Student's *t*-test, **p* < 0.05. The quantitative analysis of IHC images was reported as mean ± SD of three random areas of the tissue section. Statistical differences were calculated using a two-way ANOVA, **p* < 0.05, ***p* < 0.01, and ****p* < 0.001.

3. Results and Discussion

3.1. Alternative Model Optimization and Effects of RT and HT as Single or Combined Treatment Modalities

The efficiency of the single or combined therapy (RT, HT, and RT/HT) for the treatment of pancreatic cancer has been investigated using the optimized CAM model, an in vivo system that supports vascularized malignancies. An initial optimization of the protocol was implemented to generate solid tumors on

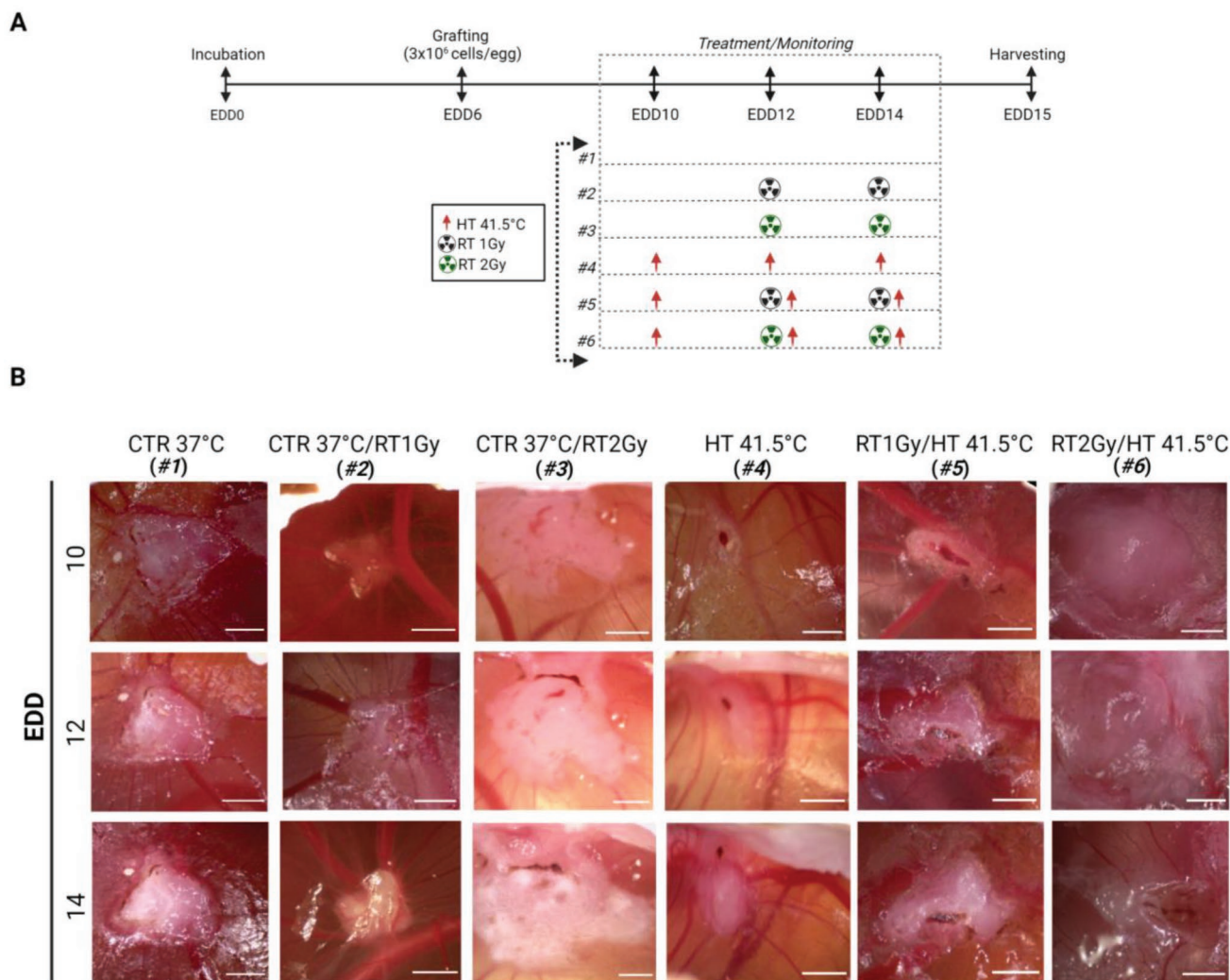


Figure 1. Treatment protocol. A) Scheme of the treatment protocol. At EDD6, 3×10^6 cells were implanted on the CAM. At EDD10, the tumor-bearing embryos were randomized and divided into six treatment groups. Radiotherapy was applied before hyperthermia in the combined treatment groups. Tumor size was monitored until EDD15. Then, tumors were harvested for further biological analysis. B) Representative images of tumors from EDD10 to 14 for the different treatment groups. Changes in the tumor consistency and vascularity (compared to the solidity of the tumor in the untreated group) highlight the efficacy of the treatments. Scale bar: 2 mm.

CAM using different numbers of BxPC-3 cells. Approximately 3×10^6 cells/egg were required for the grafting technique to generate a tumor mass on the vascularized membrane of the chicken embryo. The successful grafting percentage ($\approx 61\%$) obtained ascertained a valid biological model to allow the comparison of different treatment strategies on both viability of the embryos and tumor size. At EDD10, the tumor-bearing embryos were randomized and divided into six different groups: i) two groups received only RT at a dose of 1 and 2 Gy, respectively, on EDD12 and 14; ii) two groups received an identical RT schedule together with HT administered on EDD10, 12, and 14; and iii) two control groups comprised of a normothermic (37.5°C) and a hyperthermic (41.5°C) condition (Figure 1A). Embryo survival was not significantly affected by any treatment schedule; although, the lowest viability was recorded for the conditions HT-only and RT 1 Gy/HT as shown in the Kaplan–Meier curve (Figure S1A, Supporting Information). All treatment strategies

altered both tumor morphology and dimensions. Indeed, a visible alteration of the initial form and solidity of the tumors has been observed together with an impairment of the vascularization (Figure 1B). The volume of the tumors was estimated using a formula that considers the measurements of the width and length, as previously reported.^[13]

The volume distribution of the tumors highlights a considerable heterogeneity at EDD10 (Figure S1B, Supporting Information). Such heterogeneity can be attributed to the large variability of an *in vivo* system. The tumor volume measurements were used to derive the fold change values, in order to individually normalize the treatment groups (Figure 2A; Figure S1C, Supporting Information). No significant reduction in the average tumor volume was observed for any of the treated groups. On the other hand, a noticeable tumor-reducing effect was observed by comparing the different treatment conditions with respect to the control group (Figure 2B). Although not statistically

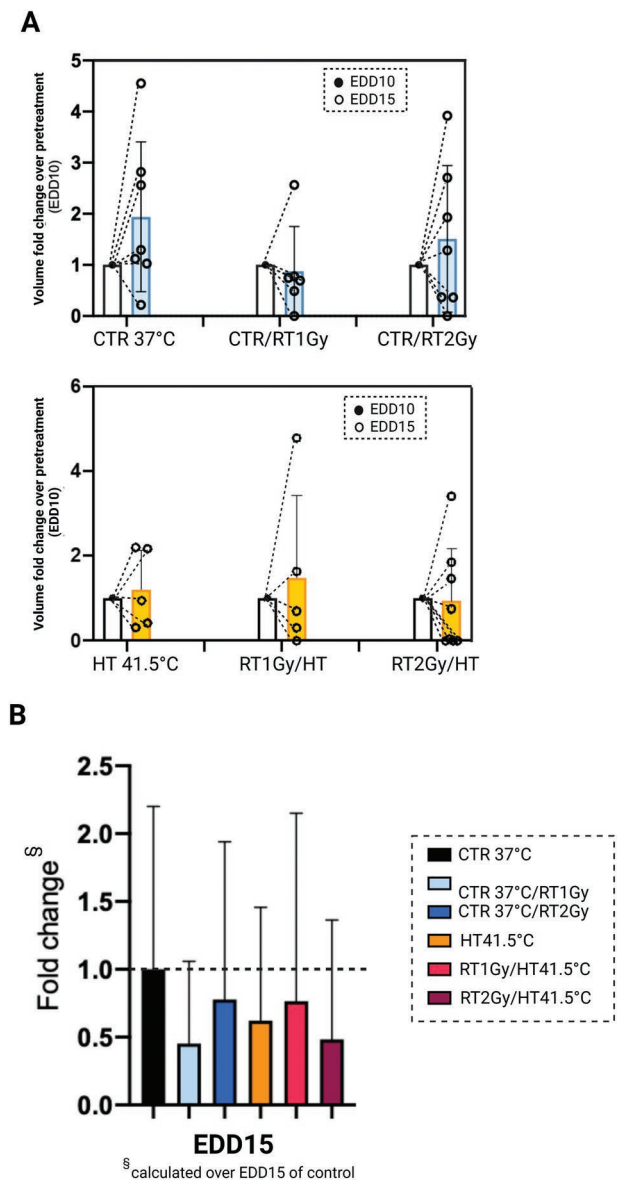


Figure 2. Effect of hyperthermia and radiotherapy in single or combined application on tumors size. A) Individual analysis for each group. Tumor volume fold change over the complete treatment course, with respect to EDD10. The data are reported as mean \pm SD (in each group, $n = 8$). B) Size-reducing effect of treatments was calculated as ratio of the average volume fold changes at EDD15 of treated eggs with respect to controls; error bars are propagation of the previously calculated SD. The dashed line refers to the fold change and it is set equal to 1. No significant statistical differences were found between treatment conditions.

significant, at EDD15, the average tumor volume for all the treatments has a ratio < 1 compared to the control (ratio equal to 1, dashed line), suggesting an overall tumor volume reduction.

3.2. Effects of the Combined Treatment Modality on the Regulation of Tumor-Promoting Mechanisms

The investigation of cancer-related mechanisms is of particular interest to evaluate the efficacy of the applied treatment and

improve the therapeutic strategy. The alteration of gene and protein expression patterns is one of the major features of cancer development process, even in its earliest stages.^[16] Hence, bio-molecular investigations were performed to assess the effects of single or combined treatments on the transcriptional regulation of certain tumor-promoting mechanisms, such as hypoxia and/or reduction/blocking of apoptosis. At EDD15, tumors were collected and processed to measure the relative amount of Carbonic Anhydrase IX (CAIX), Proliferating Cell Nuclear Antigen (PCNA), and caspase-3, which are key regulators of the hypoxia and cell cycle, respectively. Tumor hypoxia is associated with increased malignancy of cancer cells due to radiotherapy resistance and enhanced incidence of metastasis.^[17] In our study, tumors treated with only HT showed a significant reduction of CAIX expression levels, whereas greater deregulation occurred with the combined treatment approach (RT 1 or 2 Gy and HT) (Figure 3A, left). This result corroborated the role of HT in promoting both the oxygenation of the tumor tissue due to increased blood flow and vessel permeability and the tumor response when used as an adjuvant to RT, as observed in several types of tumors.^[18] For example, Brizel D.M et al. showed an improvement in the oxygenation status of soft tissue sarcoma following a combined treatment of 10–16 Gy irradiation and HT.^[19] Moreover, in human-derived head and neck tumors, an interesting therapeutic efficacy has been observed with a triple modality therapy (HT in combination with RT and CT), which markedly decreased the hypoxic area in the tumor and its respective volume.^[20]

Interesting dynamics were also observed with regard to mRNA expression levels of proliferation and apoptosis markers, i.e. PCNA and caspase-3. PCNA is a molecular target for various therapeutic strategies as it is overexpressed in pancreatic cancer and associated with a poor prognosis.^[21,22] In our investigation, tumors treated with RT 1–2 Gy/HT and RT 2 Gy alone drastically reduced the amount of PCNA mRNA (Figure 3A, middle), suggesting a reduced aggressiveness of tumors in terms of cell proliferation ability. However, this result suggests that the mRNA downregulating effect is attributed to the application of RT rather than HT, as HT alone positively regulated the PCNA gene expression. On the other hand, the mRNA levels of caspase-3 showed the same trend of PCNA for all the conditions, except for HT alone (Figure 3A, right). This finding needed further evaluation as the activation of caspase-3 implies a post-translation cleavage on the aspartate residue to exert the cell-cycle regulatory function.^[23] Therefore, IHC analysis was performed using anti-Ki67 and cleaved caspase-3 antibodies (Figure 3B, middle and right). The Aperio Software Algorithm allowed to quantify the amount of the specific staining classifying it as weak, moderate, or strong, correlating with the different degrees of the protein level. It should be noted that the different expression of PCNA and Ki67 might be attributed to their distinct role during the cell-cycle regulation.^[24] Unlike the PCNA gene, both tumors irradiated with 1 and 2 Gy showed a significant increase in Ki67 protein level compared to the control group (Figure 3C). This finding supports the accelerated cell repopulation mechanism typical for several tumor types after RT, in which the number of new dividing cells exceeds the number of lost cells.^[13,25] In fact, a marked reduction in the cleaved form of caspase-3 for the condition RT 2 Gy may

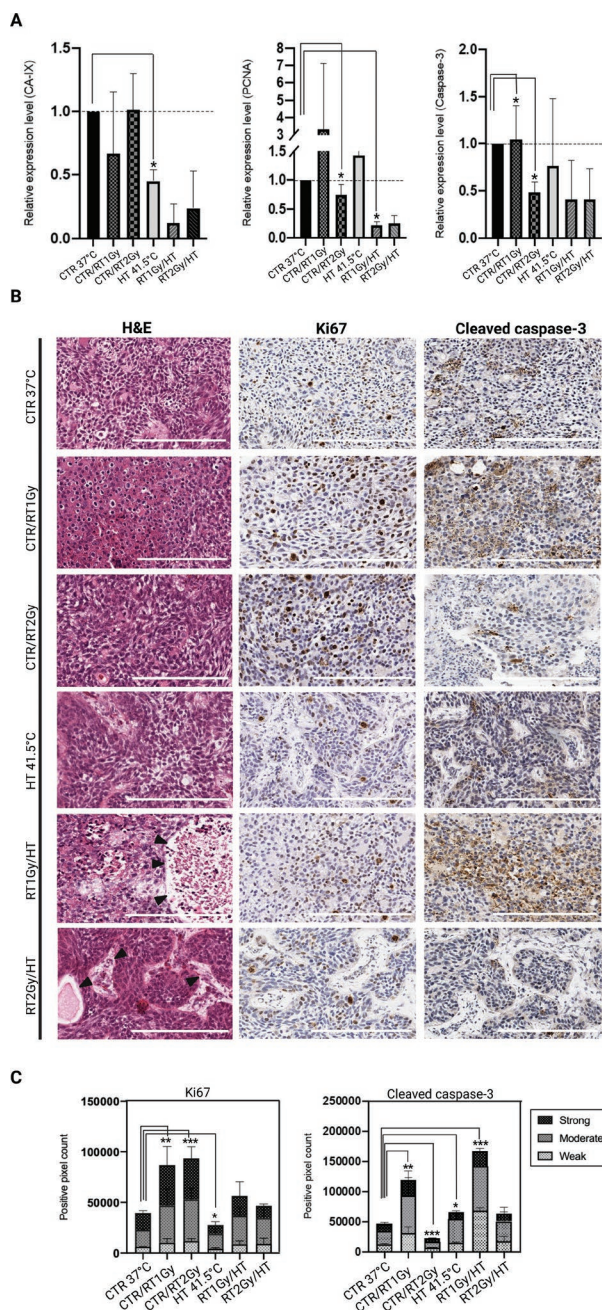


Figure 3. Evaluations of cancer promoting mechanisms. A) Comparison of CAIX (left), PCNA (middle), and caspase-3 (right) mRNA expression levels among the different treatment conditions. Data is reported as mean \pm SD for three biological replicates. Dashed lines refer to the fold change. Statistical differences were calculated through the Student's *t*-test, $*p < 0.05$. B) H&E (left) and IHC staining with anti Ki67 (middle) and cleaved caspase-3 (right) antibodies for each group of treatment. The overall architecture and cell distribution of the tumor mass is altered with the combined treatment strategies (H&E panel, black arrows). The brown signal in the IHC images of Ki67 and cleaved caspase-3 indicates proliferating and apoptotic cells, respectively. Magnification 20 \times , scale bar: 200 μ m. C) IHC images were further analyzed with Aperio Image Scope software for a quantitative evaluation of the proliferating and apoptotic cells. The positive pixel count algorithm automatically generated a scoring system based on the intensity of the positive signals (classified as weak, moderate, and strong). Statistical differences were calculated with two-way ANOVA, $*p < 0.05$, $**p < 0.01$, and $***p < 0.001$.

suggest the overall deficiency of the apoptotic mechanism. Unlike the RT 2 Gy group, tumors heated at 41.5 $^{\circ}$ C showed a significant decrease of Ki67 together with a significant increase in the active caspase-3. Interestingly, tumors from both combined treatments, RT 1 or 2 Gy and HT, showed a higher level of Ki67 compared to the HT group (Figure 3C). The Ki67 increase may be due to the contrasting effect of the accelerated cell repopulation mechanism caused by RT over the activation of apoptosis induced by HT. At the same time, this finding also infers that the use of HT as an adjuvant to RT slowed the accelerated proliferation observed in both conditions of RT alone, probably due to a marked increase in caspase-3 activation, as evidenced in tumors treated with RT 1 Gy followed by HT.

HT-induced apoptosis is a well-established mechanism observed in numerous cancer types, such as melanoma, breast cancer, colon cancer, and osteosarcoma.^[26–28] Based on the intensity and duration of the treatment, various pathways may be activated to induce cell death.^[29] For instance, treatment for 1 h at 43 $^{\circ}$ C in osteosarcoma cells triggered an increase of intracellular reactive oxygen species (ROS) and activation of caspase-3, along with endoplasmic reticulum stress and mitochondrial dysfunction.^[26] In addition, Pawlik A. et al. found that heating-induced cell death in non-small lung cancer cell line H1299 resulted from the alteration of both microtubules and mitotic spindle, which is likely correlated with apoptosis.^[30] Altogether, the result of Ki67 and cleaved caspase-3 suggests that the adjuvant effect of HT occurs through the inhibition of RT-induced accelerated proliferation along with the activation of caspase 3-dependent apoptosis.

The H&E staining revealed greater damage for tumor tissues treated with both therapies (Figure 3B, left). In fact, the impaired distribution of tumor cells in some regions highlights a loss of tissue compactness (arrow heads). Thus, the morphological alteration of tumor tissue following the combined treatment approaches further supports the adjuvant effect of HT in improving pancreatic cancer management.

The organs of the chicken embryos were examined to assess the biocompatibility and safety of the therapeutic modalities. The histological staining revealed damage of the liver and lungs in models undergoing combined RT and HT. In particular, the double treatment induced infiltration of inflammatory cells in the liver, which predominantly include lymphocytes, and necrosis of the lung tissues (Figure 4). Collectively, these results imply the need to further improve the combined therapy strategy in order to have the most effective tumor response along with minimal side effects.

3.3. Metastasis Analysis

The tumor models were also employed to evaluate the ability of the cancer cells to spontaneously metastasize in the lower CAM (L.CAM), a distal region of the grafting site. qRT-PCR enabled a quantitative analysis of the *Alu* sequences to detect intravasated human cancer cells. An increasing number of BxPC-3 cells (10 to 100.000) were added to individual homogenates of lower CAM tissue of not-grafted embryos to generate a standard curve in which the *Alu* threshold cycle (Ct_{Alu}) was plotted as function of Log_{10} of the number of cells per L.CAM

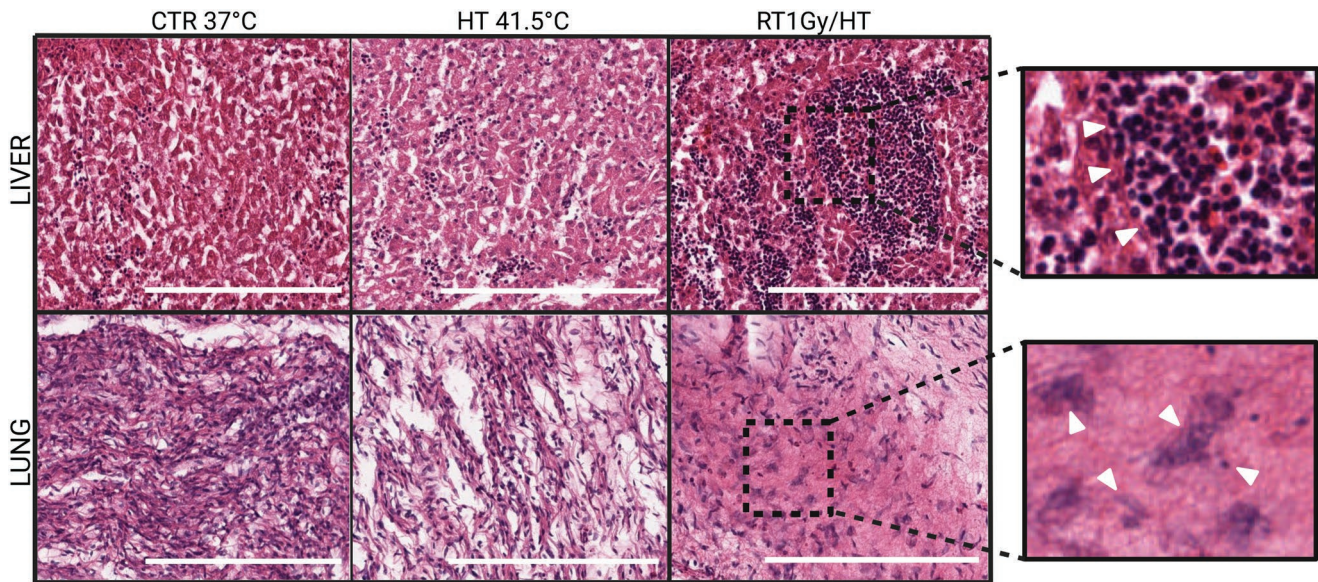


Figure 4. Biocompatibility evaluation of the combined treatment approach. Organs of the chicken embryos were harvested to assess the biocompatibility of hyperthermia in single or combined therapy. Both liver and lung showed damage that may potentially impair the normal functioning of the organs. White arrowheads in the magnified images indicate lymphocytes infiltration and disrupted nuclei (necrosis) in the liver and lung, respectively. Magnification 20 \times , scale bar: 200 μ m.

(Figure S2, Supporting Information). The minimum detectable number of cells was approximately 400 cells per L.CAM. Thus, the lower CAM tissues from the models were compared to determine the actual number of intravasated cells. In general, control tumors showed the highest metastatic potential compared to all other conditions, averaging $\approx 29 \times 10^3$ cells per tissue (Figure 5A). In contrast, tumor cells irradiated with 2 Gy dosage were not identified in any of the lower CAM samples analyzed. A comparable finding was observed in the HT and RT 2 Gy/HT conditions, where the number of intravasated cells exceeded the lower detection limit in only one sample. Hence, this initial quantitative evaluation may need further investigation to associate a potential inhibitory effect of a specific treatment strategy on the invasive property of BxPC-3 cancer cells. Indeed, the invasion-reducing effect observed by HT as a single or combined treatment might also be attributed to the initial size of the tumors. In this regard, Deryugina et al. found that the highest frequency of human cancer cells detected in the lower CAM was the result of a concomitant increased tumor size on the CAM as well as a greater number of inoculated cells.^[31] Moreover, in clinical practice, increasing tumor size affects the probability of metastasis in patients with neuroendocrine pancreatic cancer.^[32] A significant relationship between tumor dimension and metastasis was also found in patients with stage IV non-small lung carcinoma.^[33] In addition, the biological factors involved in the metastatic initiation process are not necessarily expressed by all cells originating from the primary tumor site.^[34] The heterogeneous tumor cell population with different intermediate stages of the epithelial to mesenchymal transition (EMT) may have important implication to understand the response to therapeutic treatment.^[35]

The transferrin receptor (TfR) is known to be a specific marker for cancer as it is overexpressed in malignant cells and associated with cancer progression.^[36] In this study, the

TfR was used as a marker of BxPC-3 cells to further investigate their invasive properties in the lower CAM. IHC analysis with anti-human TfR antibody confirmed the presence of intravasated human cells as dispersed foci within the mesoderm (Figure 5B). Although the lower CAM analysis provides a direct method to monitor the dissemination of tumor cells, various events are involved in the metastatic process, such as intravasation, survival in the circulation, arrest in the vasculature, extravasation, and the ability to form micro metastases in secondary organs.^[37] Thus, the applied treatment strategy to the primary tumor site might have potentially targeted one of these spontaneous events of the metastatic cascade, influencing the different invasive behavior of tumor cells of the different treatment groups.

Overall, both quantitative and qualitative analysis confirmed the colonization ability of human BxPC-3 cell line.

4. Conclusion

HT positively affected the radio-treatment in the CAM tumor model grafted with PDAC cancer cells. Despite a non-evident synergistic or combinatorial effect on the size-reduction of the neoplasms, our findings suggest promising effects on the hypoxic environment of the malignancy as well as on the remaining cellular fraction. These are encouraging findings considering the current lack of effective therapeutic strategies for pancreatic cancer. Overall, the translation of combined strategies into the clinical practice may improve the outcome for patients affected by this malignancy. In the future, further preclinical investigations regarding the application of the dual HT/RT combined with the actual standard of care (e.g., chemotherapy) for pancreatic cancer management will be evaluated. Eventually, new emerging therapies (e.g., immunotherapies

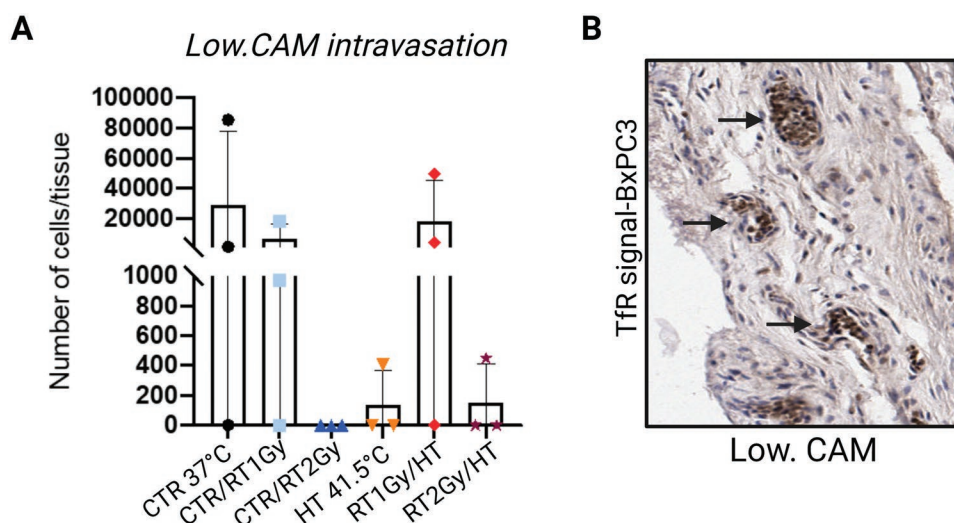


Figure 5. Intravasation behaviors of BxPC-3 cells in the lower CAM. A) Lower CAM tissues were harvested for *Alu* PCR analysis. The lower CAM from not-grafted eggs was used as a negative control and the threshold cycle (Ct) value was used as cut off for tissues from grafted eggs and exposed to different treatment approaches. Data were reported as mean \pm SD of three biological replicates. No statistical differences were found among the groups. B) Example of lower CAM tissue processed for immunohistochemistry (IHC) to further confirm the presence of BxPC-3 cells in the lower CAM by using the anti-human TFR antibody. The brown signal indicated by the arrows depicted the presence of disseminated human cells in the tissue of chicken embryo. Magnification 20 \times , scale bar: 200 μ m.

and targeted therapies) can also be evaluated using the CAM model. The employment of CAMs as *in vivo* tumor models allows to investigate effects of treatment strategies at cellular level as well as on the tumor microenvironment. Despite the great advantages of the CAM model as described, there are also a few drawbacks such as the short observation period (days), the rapid morphological changes, and the limited access to chicken antibodies for characterization. Therefore, translation of the results found in this study requires further optimization before entering any clinical stage. As continuation of this investigation, the efficacy of combined treatment strategies will be assessed on other types of neoplasms as well (e.g., head and neck carcinoma); herein, the vasodilatation induced by HT will be exploited to improve perfusion, and thereby, drug accumulation at the tumor site.

Supporting Information

Supporting Information is available from the Wiley Online Library or from the author.

Acknowledgements

The authors thanks Prof. Elisa Giovannetti for supplying the cells. Data was processed and graphs prepared by using GraphPad Prism software (version 8.0). The graphical abstract was created with BioRender.com

Open Access Funding provided by Istituto Italiano di Tecnologia within the CRUI-CARE Agreement.

Conflict of Interest

The authors T.L., L.B., E.v.Z., J.V.d.B., and J.B. are directly or indirectly employed by ElmediX NV, a Belgian spinoff of the University of Antwerp

(Belgium), developing a device for WBH. The authors J.V.D.B. and J.B. are co-founders of ElmediX NV and direct or indirect shareholders. The other authors declare no competing financial interests that could have appeared to influence the work reported in this paper.

Author Contributions

In vivo experiments: P.S., A.Z., A.K.M., N.G., and A.G. *Biological analysis:* P.S. and A.Z. *Irradiation experiments:* N.G., A.G., and S.L. *Histological analysis:* M.M. *Data analysis:* T.L., L.B., E.v.Z., R.C., J.V.d.B., and J.B. *Project design and coordination:* V.V. All Authors have discussed the data and contributed to write the manuscript.

Data Availability Statement

The data that support the findings of this study are available from the corresponding author upon reasonable request.

Keywords

combined treatments, hyperthermia, oncology, pancreatic carcinoma, radiotherapy

Received: August 21, 2022

Revised: December 19, 2022

Published online:

- [1] P. Rawla, T. Sunkara, V. Gaduputi, *World J. Oncol* **2019**, *10*, 10.
- [2] M. S. D. De La Cruz, A. P. Young, I. V. M. T Ruffin, *Am. Fam. Physician* **2014**, *89*, 626.
- [3] S. Mohammed, G. Van Buren, W. E. Fisher, *World J. Gastroenterol.* **2014**, *20*, 9354.

- [4] V. Jiang, D. P. S. Sohal, *JCO Oncol. Pract.* **2023**, 19, 19.
- [5] S. Chand, K. O'hayer, F. F. Blanco, J. M. Winter, J. R. Brody, *Int. J. Biol. Sci.* **2016**, 12, 273.
- [6] M. C. Bosco, G. D'Orazi, D. Del Bufalo, *J. Exp. Clin. Cancer Res.* **2020**, 39, 8.
- [7] B. Wylleman, L. Brancato, I. Gorbaslieva, E. Van Zwol, M. G. M. C. Mori Da Cunha, J. Benoit, D. Tierny, P. Vueghs, J. Van Den Bossche, O. Rudenko, M. Janicot, J. Bogers, *Int. J. Hyperthermia* **2022**, 39, 48.
- [8] H. P. Kok, E. N. K. Cressman, W. Ceelen, C. L. Brace, R. Ivkov, H. Grüll, G. Ter Haar, P. Wust, J. Crezee, *Int. J. Hyperthermia* **2020**, 37, 711.
- [9] A. K. Mapanao, P. P. Che, P. Sarogni, P. Sminia, E. Giovannetti, V. Voliani, *Expert Opin. Drug Metab. Toxicol.* **2021**, 17, 947.
- [10] A. Vargas, M. Zeisserlabouebe, N. Lange, R. Gurny, F. Delie, *Adv. Drug Delivery Rev.* **2007**, 59, 1162.
- [11] H. Chen, C. S. Wang, M. Li, E. Sanchez, J. Li, A. Berenson, E. Wirtschafter, J. Wang, J. Shen, Z. Li, *BB and JRB. Int. J. Oncol.* **2010**, 37, 71.
- [12] T. Wang, S. Chen, S. Wang, L. Shi, C. Wang, J. Zhang, Y. Gao, G. Li, Y. Qi, X. An, L. Chen, *OncoTargets Ther.* **2017**, 8, 40713.
- [13] P. Sarogni, A. K. Mapanao, A. Gonnelli, M. L. Ermini, S. Marchetti, C. Kusmic, F. Paiar, V. Voliani, *iScience* **2022**, 25, 103980.
- [14] P. Sarogni, A. K. Mapanao, S. Marchetti, C. Kusmic, V. Voliani, *ACS Pharmacol. Transl. Sci.* **2021**, 4, 1227.
- [15] K. J. Livak, T. D. Schmittgen, *Methods* **2001**, 25, 402.
- [16] C. Garnis, T. P. Buys, W. L. Lam, *Mol Cancer* **3** **2004**, 9, <https://doi.org/10.1186/1476-4598-3-9>.
- [17] W. Boulefour, E. Rowinski, S. Louati, S. Sotton, A.-S. Wozny, P. Moreno-Acosta, B. Mery, C. Rodriguez-Lafrasse, N. Magne, *Med. Sci. Monit.* **2021**, 27, e934116.
- [18] A. Van Der Horst, E. Versteijne, M. G. H. Besselink, J. G. Daams, E. B. Bulle, M. F. Bijlsma, J. W. Wilminck, O. M. Van Delden, J. E. Van Hooft, N. A. P. Franken, H. W. M. Van Laarhoven, J. Crezee, G. Van Tienhoven, *Int. J. Hyperthermia* **2017**, 34, 969.
- [19] D. M. Brizel, S. P. Scully, J. M. Harrelson, L. J. Layfield, R. K. Dodge, H. C. Charles, T. V. Samulski, L. R. Prosnitz, M. W. Dewhirst, *Cancer Res.* **1996**, 56, 5347.
- [20] A. Ressel, C. Weiss, T. Feyerabend, *Int. J. Radiat. Oncol. Biol. Phys.* **2001**, 49, 1119.
- [21] S. J. Smith, C. M. Li, R. G. Lingeman, R. J. Hickey, Y. Liu, L. H. Malkas, M. Raof, *Mol. Ther. Oncolytics* **2020**, 17, 250.
- [22] K. L. Dillehay, S. Lu, Z. Dong, *Mol. Cancer Ther.* **2014**, 13, 2817.
- [23] Y. Shi, *Mol. Cell* **2002**, 9, 459.
- [24] R. Bologna-Molina, A. Mosqueda-Taylor, N. Molina-Frechero, Ad. Mori-Estevez, G. Sanchez-Acuna, *Med Oral Patol Oral Cir Bucal* **2013**, 18, e174.
- [25] S. S. Yom, *Semin. Radiat. Oncol.* **2015**, 25, 93.
- [26] C. -H. Hou, F. -L. Lin, S. -M. Hou, J. -F. Liu, *Int. J. Mol. Sci.* **2014**, 15, 17380.
- [27] Y. G. Shellman, W. R. Howe, L. A. Miller, N. B. Goldstein, T. R. Pacheco, R. L. Mahajan, S. M. Larue, D. A. Norris, *J. Invest. Dermatol.* **2007**, 128, 949.
- [28] F. Chen, C. Wang, E. Kim, L. Harrison, *Cell Biol. Int.* **2008**, 32, 715.
- [29] K. Ahmed, Y. Tabuchi, T. Kondo, *Apoptosis* **2015**, 20, 1411.
- [30] A. Pawlik, J. M. Nowak, D. Grzanka, L. Gackowska, J. Michalkiewicz, A. Grzanka, *Acta Histochem.* **2013**, 115, 8.
- [31] E. I. Deryugina, A. Zijlstra, J. J. Partridge, T. A. Kupriyanova, M. A. Madsen, T. Papagiannakopoulos, J. P. Quigley, *Cancer Res.* **2005**, 65, 10959.
- [32] Y. Liu, S. Ye, Y. Zhu, X. He, J. Pan, S. Chen, B. Ye, L. Wang, *J. Cancer* **2019**, 10, 6349.
- [33] Q. Shan, Y. Fan, J. Guo, X. Han, H. Wang, Z. Wang, *PeerJ* **2019**, 2019, 1.
- [34] J. Fares, M. Y. Fares, H. H. Khachfe, H. A. Salhab, Y. Fares, *Signal Transduction Targeted Ther.* **2020**, 5, 28.
- [35] I. Pastushenko, A. Brisebarre, A. Sifrim, M. Fioramonti, T. Revenco, S. Boumahdi, A. Van Keymeulen, D. Brown, V. Moers, S. Lemaire, S. De Clercq, E. Minguijón, C. Balsat, Y. Sokolow, C. Dubois, F. De Cock, S. Scozzaro, F. Sopena, A. Lanas, N. D'haene, I. Salmon, J. - C. Marine, T. Voet, P. A. Sotiropoulou, C. Blanpain, *Nature* **2018**, 556, 463.
- [36] E. R. Camp, C. Wang, E. C. Little, P. M. Watson, K. F. Pirollo, *Bone* **2013**, 20, 222.
- [37] A. Zijlstra, R. Mellor, G. Panzarella, R. T. Aimes, J. D. Hooper, N. D. Marchenko, J. P. Quigley, *Cancer Res.* **2002**, 62, 7083.
- [38] M. Santi, V. Frusca, M. L. Ermini, A. K. Mapanao, P. Sarogni, A. Gonnelli, N. Giannini, A. Zamborlin, L. Biancalana, F. Marchetti, V. Voliani, (2023), Hybrid nano-architectures loaded with metal complexes for the co-chemotherapy of head and neck carcinomas. *Journal of Materials Chemistry B*, 11(2), 325–334. <https://doi.org/10.1039/d2tb01930b>.
- [39] A. K. Mapanao, P. Sarogni, M. Santi, M. Menicagli, A. Gonnelli, A. Zamborlin, M. L. Ermini, V. Voliani, (2022), Pro-apoptotic and size-reducing effects of protein corona-modulating nano-architectures enclosing platinum prodrug in in vivo oral carcinoma. *Biomaterials Science*, 10(21), 6135–6145. <https://doi.org/10.1039/d2bm00994c>.